High Performance All-Polymer Solar Cells by Synergistic Effects of Fine-Tuned Crystallinity and Solvent Annealing

Zhaojun Li,[†] Xiaofeng Xu,*[,†] Wei Zhang,[‡] Xiangyi Meng,[§] Wei Ma,[§] Arkady Yartsev,[‡] Olle Inganäs,[∥] Mats. R. Andersson,[⊥] René A. J. Janssen,*[,#] and Ergang Wang*[,†]

[†]Department of Chemistry and Chemical Engineering, Chalmers University of Technology, SE-412 96 Göteborg, Sweden
[‡]Division of Chemical Physics, Lund University, Box 124, 221 00 Lund, Sweden
[§]State Key Laboratory for Mechanical Behavior of Materials, Xi'an Jiaotong University, Xi'an 710049, China
[∥]Biomolecular and Organic Electronics, IFM, Linköping University, SE-581 83 Linköping, Sweden
[⊥]Future Industries Institute, University of South Australia, Mawson Lakes Boulevard, Mawson Lakes, SA 5095, Australia
[#]Molecular Materials and Nanosystems and Institute for Complex Molecular Systems, Eindhoven University of Technology, PO BOX 513, 5600 MB Eindhoven, The Netherlands

S *Supporting Information*
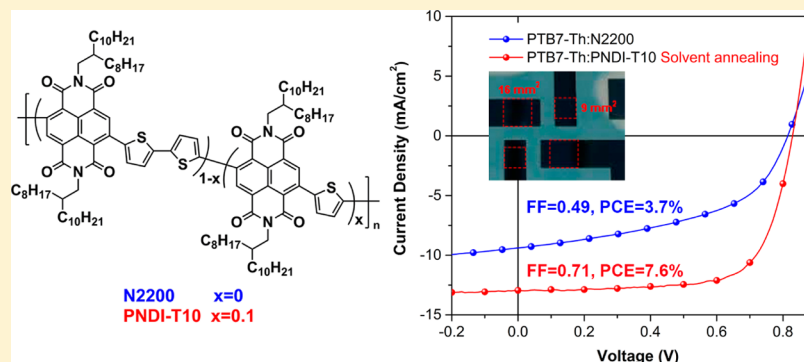
ABSTRACT: Growing interests have been devoted to the design of polymer acceptors as potential replacement for fullerene derivatives for high-performance all polymer solar cells (all-PSCs). One key factor that is limiting the efficiency of all-PSCs is the low fill factor (FF) (normally <0.65), which is strongly correlated with the mobility and film morphology of polymer:polymer blends. In this work, we find a facile method to modulate the crystallinity of the well-known naphthalene diimide (NDI) based polymer N2200, by replacing a certain amount of bithiophene (2T) units in the N2200 backbone by single thiophene (T) units and synthesizing a series of random polymers PNDI-Tx, where x is the percentage of the single T. The acceptor PNDI-T10 is properly miscible with the low band gap donor polymer PTB7-Th, and the nanostructured blend promotes efficient exciton dissociation and charge transport. Solvent annealing (SA) enables higher hole and electron mobilities, and further suppresses the bimolecular recombination. As expected, the PTB7-Th:PNDI-T10 solar cells attain a high PCE of 7.6%, which is a 2-fold increase compared to that of PTB7-Th:N2200 solar cells. The FF of 0.71 reaches the highest value among all-PSCs to date. Our work demonstrates a rational design for fine-tuned crystallinity of polymer acceptors, and reveals the high potential of all-PSCs through structure and morphology engineering of semicrystalline polymer:polymer blends.

INTRODUCTION

Polymer solar cells (PSCs) have attracted considerable attention in recent years due to their unique advantages of being flexible, lightweight, and the ability to be manufactured on a large-area scale at low cost.[1] The bulk-heterojunction (BHJ) PSCs, incorporating a solution-processed conjugated polymer and a fullerene derivative, have been widely studied in the past decades.[2] Considerable progress has been made in these fullerene-based PSCs, and the power conversion efficiency (PCE) of single-junction PSCs have attained 11%.[3] On the other hand, all polymer solar cells (all-PSCs), using a *p*-type polymer and an *n*-type polymer in a blend, processed from

solution for active layer fabrication, have attracted much less attention until recently.[4] Compared to fullerene derivatives, *n*-type polymers offer unique attractions owing to the low cost, strong light absorption at near-infrared wavelengths and good thermal stabilities.[5] Moreover, the molecular weights, absorption spectra, band gaps and molecular orientation of both *n*-type acceptor and *p*-type donor polymers can be well matched by rational design, suggesting intriguing opportunities for enhancing efficiency.[6] Up to date, the efficiency of all-PSCs is

Scheme 1. Chemical Structures of Donor and Acceptor Polymers

PTB7-Th   N2200   x=0.1, PNDI-T10
PNDI-Tx x=0.2, PNDI-T20
x=0.5, PNDI-T50

still behind that of fullerene-based PSCs. Therefore, more research efforts need to be devoted to the development of new *n*-type polymer acceptors. Similar to the design of donor polymers, a facile method for the synthesis of polymer acceptors is to combine an electron-donating (D) and an electron-withdrawing (A) moiety alternately. For example, strong A units including 2,1,3-benzothiadiazole (BT),[7] diketopyrrolopyrrole (DPP),[8] naphthalene diimide (NDI)[9] and perylene diimide (PDI)[10] have been incorporated with strong D units to afford various acceptor polymers. An appealing acceptor polymer is poly[[*N*,*N*′-bis(2-octyldodecyl)-naphthalene-1,4,5,8-bis(dicarboximide)-2,6-diyl]-*alt*-5,5′-(2,2′-bithiophene)] with the commercial name N2200, which provides high electron affinity, electron mobility, good solubility and strong absorption in the visible and near-infrared region.[11] These characteristics have enabled advances in N2200-based all-PSCs. The efficiency of poly[4,8-bis[5-(2-ethylhexyl)-2-thienyl]benzo[1,2-*b*:4,5-*b*′]dithiophene-*alt*-(4-(2-ethylhexyl)-3-fluorothieno[3,4-*b*]thiophene-)-2-carboxylate-2-6-diyl)] (PTB7-Th):N2200-based all-PSCs has been steadily improving to 5.7%.[12] Very recently, a maximal PCE of 8.27% has been reached by using a more absorption-complementary polymer donor with N2200 as the acceptor.[5a] One key factor that is limiting the efficiency of all-PSCs is the low fill factor (FF) (normally <0.65), which is largely correlated to the suboptimal morphology, low and unbalanced hole and electron mobility. The N2200 polymer can easily form large crystals in polymer:N2200 blends due to the rigid and planar structures of NDI units, which leads to large domain sizes and phase separation.[13] Therefore, controlling the polymer crystallization, molecular ordering and scale of phase separation is essential for N2200-based all-PSCs. The nanostructure of polymer:N2200 blends can be influenced via polymer/solvent and polymer/additive interactions, and the thermal properties of both the donor polymer and N2200. Hence both the film deposition and post-treatment procedures are commonly varied for different polymer:N2200 combinations to enhance device performance.[14] Moreover, there was evidence that the use of flexible moieties or side chains modulation of NDI-based polymers can lead to tunable crystallinity and suitable miscibility.[15] For these reasons, developing rational methods to better control the flexibility of N2200 backbone and nanostructure of such donor polymer:N2200 blends can have a major impact on the overall performance.

Inspired by the strategies, we introduced a certain amount of single thiophene (T) units to replace the bithiophene (2T) units as electron-donating units in the N2200 backbone, and synthesized a series of random polymers PNDI-T*x* (*x* stands for the percentage of single thiophenes relative to total donor units). The molar percentage of thiophene was 10%, 20% and 50% (Scheme 1 and Scheme S1). The random polymers are expected to have more flexible backbones and lower crystallinity due to their reduced regularity in the main chain. The polymer PTB7-Th was selected as the electron donor material in this work, since the blend of PTB7-Th:N2200 has shown very promising properties with high photovoltaic performance.[12] We have conducted a systematic study on the absorption, energy levels, crystallinity, film morphology, exciton dissociation and charge transport of the PTB7-Th:PNDI-T*x* and PTB7-Th:N2200 blends, and correlated the polymer structures to the photovoltaic performance. Compared to N2200, PNDI-T10 shows the desired nanoscale blend morphology with balanced hole and electron mobilities and reduced bimolecular recombination, which leads to a high PCE of 7.6% with a high short-circuit current density (J_{sc}) of 12.9 mA/cm^2 and a record FF of 0.71. This FF reaches the highest value among all-PSCs, approaching to the FF of 0.74 in the record-efficient PTB7-Th/PC$_{71}$BM PSCs.[16] The PCE is among the highest efficiencies of all-PSCs using the PTB7-Th donor and NDI-based acceptors.

■ RESULTS AND DISCUSSION

The random polymers PNDI-T*x* were synthesized by Stille coupling polymerization of three monomers, 2,6-dibromonaphthalene-1,4,5,8-tetracarboxylic-*N*,*N*′-bis(2-octyldodecyl)diimide (NDIBr$_2$), 5,5′-bis(trimethylstannyl)-2,2′-bithiophene (2T), and 2,5-bis(trimethylstannyl)thiophene (T). All the polymers represent good solubility in common organic solvents, like chloroform (CF), chlorobenzene (CB), and *o*-dichlorobenzene (*o*DCB) at room temperature. The molecular weights of the polymers were measured via gel permeation chromatography (GPC) in 1,2,4-trichlorobenzene at 150 °C. As summarized in Table 1, the N2200 polymer has the lowest number-average molecular weight (M_n) of 30.5 kDa with a polydispersity index (PDI) of 3.8. On the other hand, the random polymers PNDI-T10 and PNDI-T20 show much higher M_n of 66.6 kDa and 67.7 kDa, respectively, which is ascribed to the introduction of disorder and thus improved solubility. Polymer PNDI-T50 has a lower M_n of 41.9 kDa compared to PNDI-T10 and PNDI-

Table 1. Molecular Weight, Thermal Transition and Optical Properties of Polymer PNDI-T*x* and N2200

polymer	M_n (kDa)	PDI	T_m (°C)	T_c (°C)	ΔH_m (J/g)	λ_{max} (nm)	E_g^{opt} (eV)
PTB7-Th	35.0	3.0	–	–	–	700	1.60
N2200	30.5	3.8	305	280	18.3	698	1.44
PNDI-T10	66.6	5.0	290	267	11.9	694	1.55
PNDI-T20	67.7	5.0	266	236	8.6	680	1.56
PNDI-T50	41.9	3.1	227	206	7.6	644	1.60

T20. This might be caused by the increased steric hindrance between neighboring NDI units while increasing the fraction of thiophene moieties. The introduction of disorder turns out to be a facile method to increase molecular weights of polymers and thus potentially benefit their photovoltaic performance.

Differential scanning calorimetry (DSC) was employed to determine the solid-state thermal transitions. The DSC curves are depicted in Figure 1 and the thermal transition parameters
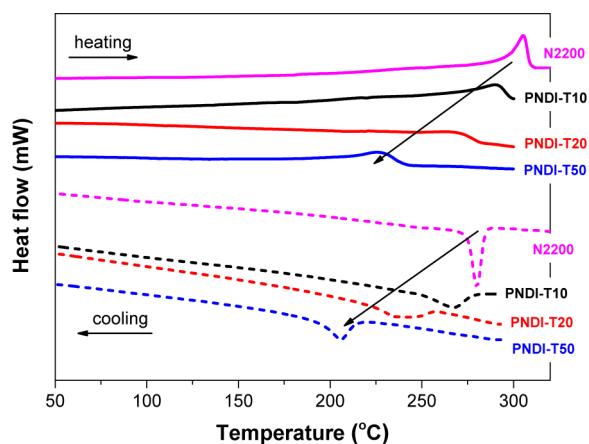
Figure 1. DSC thermograms of neat PNDI-T*x* and N2200, measured with a scan rate of 10 °C per minute.

are summarized in Table 1. All acceptor polymers present a clear melting transition upon heating and a crystallization transition upon cooling, but the glass transition is not detectable by DSC. The melting temperature (T_m) of N2200

is as high as 305 °C, which is a relatively high value among conjugated polymers. Inclusion of single thiophene units in the backbone gradually reduces the T_m and crystallization temperature (T_c) of the polymers. This indicates that the rigidity or/ and chain stacking of the polymers is weakened due to the increased backbone disorder. The area of the melting peak provides the specific melting enthalpy of samples, ΔH_m, which is strongly correlated to the crystallinity.[17] The N2200 polymer shows the highest ΔH_m of 18.3 J/g, and the value drops to 11.9 J/g for PNDI-T10 and 8.6 J/g for PNDI-T20, while PNDI-T50 shows the lowest ΔH_m of 7.6 J/g. The variations in melting enthalpy are consistent with the trends of T_m and T_c. It implies that the crystallinity of the polymers is gradually reduced due to the inclusion of disorder in the backbones.[18] The neat PTB7-Th polymer does not show any obvious thermal transitions (Figure S1 in SI). Likewise, no obvious thermal transition is observed for the blend films (Figure S1 in SI), indicating that the two polymers in each blend can be well-mixed and large crystals of the acceptor polymers are not present in the blends. The thermal transition properties of the random polymers agree well with our expectation and confirm our design motif.

The optical absorption properties of the donor PTB7-Th and the acceptors PNDI-T*x* and N2200 were characterized via UV−vis−NIR absorption spectroscopy. As depicted in Figure. 2a and Figure S2a in SI, the absorption spectra of PNDI-T*x* in thin films are red-shifted compared to those in solutions, due to $\pi-\pi$ stacking and intermolecular interactions in the solid state.[13] PNDI-T*x* and N2200 show two distinct absorption bands at 300−400 nm and 500−700 nm, which arise from excitations with the $\pi-\pi^*$ manifold, and is corresponding to transitions with local NDI and intramolecular charge transfer (ICT) character, respectively.[13,19] For N2200, the absorption maximum (λ_{max}) of the ICT $\pi-\pi^*$ band is around 694 nm. Increasing the fraction of thiophenes results in a gradual blue shift of the λ_{max} of the ICT $\pi-\pi^*$ band, from 694 nm in PNDI-T10 to 644 nm in PNDI-T50.[12c] The absorption coefficients of the polymer ICT absorption bands are around 15−22 $Lg^{-1}cm^{-1}$ in solution (Figure S2b in SI). The absorption coefficients of the polymers in thin films are included in Figure S2c in SI, which represent little difference in intensity for all the acceptor polymers.

The electrochemical properties of the polymers and $PC_{71}BM$ were measured using square wave voltammetry (SWV) (Figure S3 in SI). As depicted in the energy diagram (Figure 2b), the
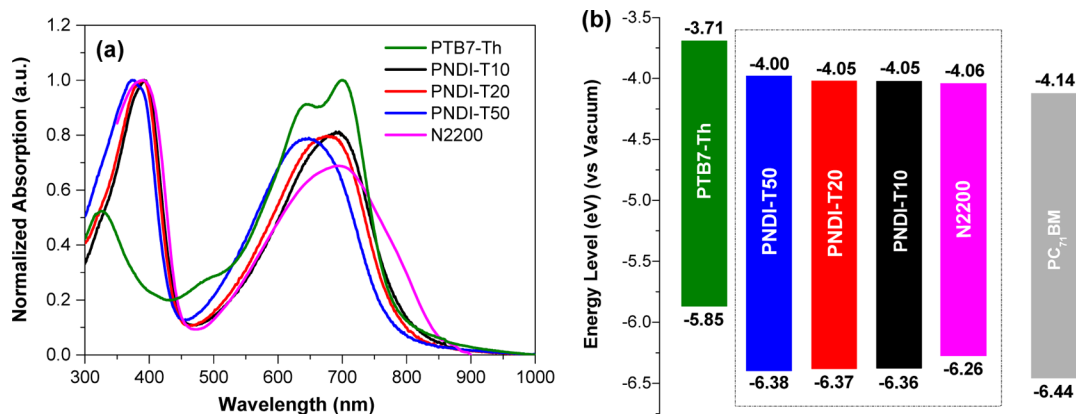
Figure 2. (a) UV−vis−NIR absorption spectra of PTB7-Th, N2200 and PNDI-T*x* in films; (b) energy levels of PTB7-Th, PNDI-T*x*, N2200 and $PC_{71}BM$.

Table 2. Photovoltaic Parameters of the Optimized PTB7-Th:PNDI-T*x* and PTB7-Th:N2200 Solar Cells

donor:acceptor	V_{oc} (V)	J_{sc} (mA/cm^2)	FF	PCE (%)	SCLC μ_h (cm^2 V^{-1} s^{-1})	SCLC μ_e (cm^2 V^{-1} s^{-1})	μ_h/μ_e
PTB7-Th:N2200	0.81	9.4 (8.7)[b]	0.49	3.7[3.4][c]	2.0×10^{-3}	2.0×10^{-4}	10
PTB7-Th:PNDI-T10	0.82	12.7 (12.4)	0.54	5.6[5.5]	8.5×10^{-4}	4.3×10^{-4}	2
PTB7-Th:PNDI-T10 SA[a]	0.83	12.9 (12.5)	0.71	7.6[7.4]	1.0×10^{-3}	6.0×10^{-4}	1.7
PTB7-Th:PNDI-T20	0.83	9.7 (9.2)	0.52	4.2[4.1]	8.4×10^{-4}	1.4×10^{-4}	6
PTB7-Th:PNDI-T50	0.83	5.8 (5.2)	0.48	2.3[2.1]	8.2×10^{-4}	9.5×10^{-5}	9

[a]Solvent annealing. [b]The photocurrents obtained by integrating the EQE with the AM1.5G spectrum are given between parentheses. [c]Average PCE of ten devices.
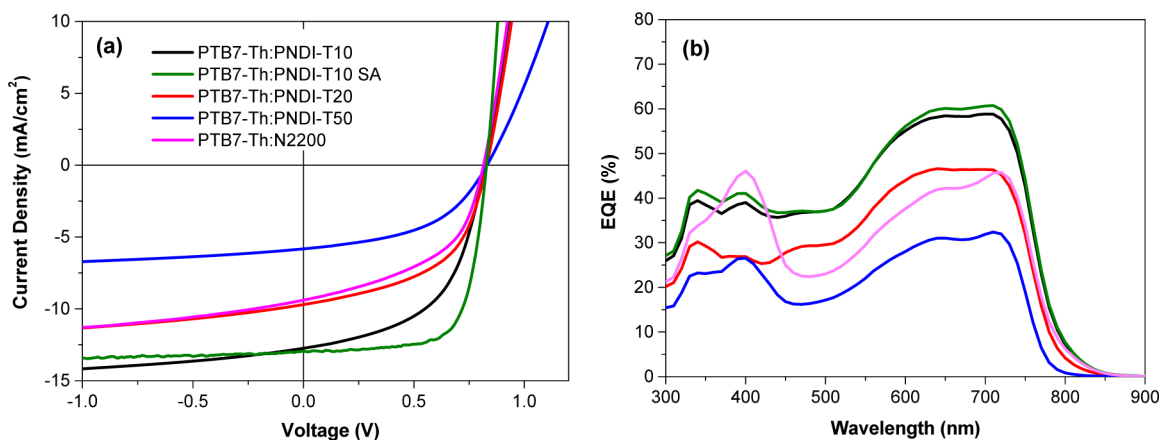
Figure 3. (a) *J*−*V* characteristics of PTB7-Th:PNDI-T*x* (1:1 w:w) and PTB7-Th:N2200 (1:1 w:w) solar cells; (b) Corresponding EQE spectra measured under 100 mW/cm^2 AM 1.5G solar illumination.

highest occupied molecular orbital (HOMO) of the three random polymers are lowered by ca. 0.1 eV compared to the level of N2200 and are close to that of PC$_{71}$BM. N2200 and the three random polymers show similar lowest unoccupied molecular orbital (LUMO) levels around −4.05 eV, which stems from the dominant contribution of the electron-withdrawing NDI units. The up-lying LUMO levels of the polymer acceptors compared to PC$_{71}$BM are in favor of providing higher V_{oc} of the all-PSCs.[20] The HOMO and LUMO levels of PTB7-Th are −5.85 eV and −3.71 eV, respectively. Each combination of the PTB7-Th donor and the NDI-based acceptor provides sufficient energy offsets (>0.3 eV) for efficient exciton dissociation in the polymer:polymer blends.[21]

All-PSCs with a conventional configuration of ITO/PEDOT:PSS/PTB7-Th:acceptor/LiF/Al were employed to evaluate the acceptor polymers. Measurements of photovoltaic performance were carried out under an illumination of AM 1.5G simulated solar light at 100 mW/cm^2. The optimized ratios of PTB7-Th:PNDI-T*x* and PTB7-Th:N2200 were 1:1 (w:w), and the optimized film thicknesses of the active layers, which were spin-coated from CB solutions (Table S1a in SI), were around 95 nm. The corresponding all-PSC parameters are summarized in Table 2, and the current density−voltage (*J*−*V*) curves are depicted in Figure 3a. The PTB7-Th:N2200 solar cell shows a PCE of 3.7% with a V_{oc} of 0.81 V, J_{sc} of 9.4 mA/cm^2 and FF of 0.49. The performance is in good agreement with the reports of PTB7-Th:N2200 solar cells using the same device configuration and procedure.[14a,22] Compared to the PTB7-Th:N2200 solar cells, the performance of PTB7-Th:PNDI-T10 solar cells is significantly enhanced and attains a PCE of 5.6% with a higher J_{sc} of 12.7 mA/cm^2, and a FF of 0.54. In the PTB7-Th:PNDI-T20 solar cell, a J_{sc} of 9.7 mA/cm^2 and a FF of 0.52 is observed with a modest PCE of 4.2%. The

PTB7-Th:PNDI-T50 solar cell shows the lowest J_{sc}, FF, and PCE. The PTB7-Th:PNDI-T*x* solar cells present slightly higher V_{oc} compared to PTB7-Th:PC$_{71}$BM solar cells due to the higher LUMO levels of the polymer acceptors.[16] The enhanced efficiency of PTB7-Th:PNDI-T10 solar cells suggest that inclusion of small amount of thiophene in the N2200 backbone affords a better counterpart for the PTB7-Th donor. For systematic optimization, several approaches have been carried out to control the morphology of PTB7-Th:PNDI-T10 solar cells. Thermal annealing at 80 °C for 10 min and the use of processing additive 1,8-diiodooctane (DIO) were found to have negative influence on the device performance (Table S1c in SI). In contrast, solvent annealing (SA) turns out to be an effective method to improve the device performance (Table S1d in SI). Upon SA, well-organized nanostructures can be formed by controlling the rate of the solvent evaporation, which is seldom used for polymer:polymer blends until very recently.[23] In our case, it enables the PTB7-Th:PNDI-T10 films to dry very slowly and both polymers have very long time for molecular rearrangement. SA of PTB7-Th:PNDI-T10 solar cell with CB leads to a remarkable increase in FF from 0.54 to 0.71 without notable change in V_{oc} and J_{sc}. It is among the highest FF in all-PSCs, which approaches that of 0.74 in the record-efficient PTB7-Th:PC$_{71}$BM solar cells.[16] The average PCE from ten solar cells was calculated to be 7.4% (Table S1e in SI). The best performing solar cell attains a PCE of 7.6%, which is among the highest efficiencies of PTB7-Th and NDI-based all-PSCs. It is worth noting that the high efficiency was readily reproduced for two different active areas (9 and 16 mm^2) as depicted in Figure S4 in SI. To verify the efficiency, we independently fabricated the all-PSCs at both Eindhoven University of Technology and Linkoping University and obtained similar results. To our knowledge, this is the highest efficiency in all-PSCs certified in different laboratories, using a device area over 10 mm^2. For

PTB7-Th:N2200 solar cells, SA has no obvious influence on the photovoltaic performance. This is probably because the polymer chains of N2200 can assemble in a very short time due to its rigid and highly regioregular backbones. Therefore, the extension of time for crystallization has no obvious influence on its morphology.[14f] In addition, there was evidence indicating that poly[[N,N′-bis(2-octyldodecyl)-naphthalene-1,4,5,8-bis-(dicarboximide)-2,6-diyl]-alt-5,5′-thiophene] (PNDI-T) is another promising NDI-based polymer acceptor.[24] In this work, we also synthesized this polymer and used it as acceptor for comparison with other NDI-based polymers. The PTB7-Th:PNDI-T all-PSC gives a PCE of 3.1% with a V_{oc} of 0.82 V, J_{sc} of 9.1 mA/cm^2 and FF of 0.42. Since PNDI-T10 has only 10% of thiophene units in the backbone, its structure is more similar to N2200 rather than PNDI-T. Therefore, there is no detailed characterization and comparison for PNDI-T included in this work.

To investigate the influence of molecular weights on the performance, another batch of PNDI-T10 with lower M_n of 60.0 kDa was synthesized. After SA, this polymer gives a PCE of 6.5% with a V_{oc} of 0.83 V, J_{sc} of 10.8 mA/cm^2 and FF of 0.73, which is slightly lower than that of the high molecular weight batch. This observation agrees well with the previous reports,[6c,d] and also indicates that the higher molecular weight of the random copolymer contributes to the higher photovoltaic performance.

The external quantum efficiency (EQE) was measured to evaluate the spectral response of the all-PSCs and the accuracy of the photocurrents in the J−V measurements. As shown in Figure 3b, the EQE curves show photoresponse over the region between 300 and 850 nm, consistent with the absorption spectra of PTB7-Th:PNDI-Tx and PTB7-Th:N2200 blend films and corroborating the contribution to photocurrent from both donor and acceptor polymers. The PTB7-Th:PNDI-T10 solar cell shows the highest photoresponse with an EQE exceeding 50% in the range of 600−750 nm. The influence of SA on the absorption spectra of the neat PTB7-Th, neat PNDI-T10 and PTB7-Th:PNDI-T10 blend films were evaluated as depicted in Figure S2d in SI. The unchanged absorption spectrum after SA agrees well with its EQE profile and the measured J_{sc}. The J_{sc} values calculated from the EQE curves are slightly lower than the measured J_{sc} from the J−V curves with a mismatch of less than 8%.

To characterize the charge transport in detail, we investigated the charge carrier mobilities in the blends using space charge limited current (SCLC) measurements in hole-only and electron-only device configurations. The corresponding J−V characteristics and SCLC fits are shown in Figure S5 in SI and the hole and electron mobilities are summarized in Table 2. The PTB7-Th:PNDI-Tx blends possess lower hole mobilities compared to the PTB7-Th:N2200 blend. The differences are fairly small and the fact that hole mobility of PTB7-Th varies by a factor of 2.5 in these blends signifies that morphological effects play a role. With respect to the electron transport, we find that introduction of more disorder in the polymer backbone, i.e. going from PNDI-T20 to PNDI-T50, lowers the electron mobility. The slightly higher electron mobility of PTB7-Th:PNDI-T10 compared to PTB7-Th:N2200 is likely related to its much higher molecular weight of PNDI-T10 which often enhances the mobility of conjugated polymers.[25] By a slightly decreased hole mobility and enhanced electron mobility, the PTB7-Th:PNDI-T10 blend reaches a more balanced μ_h/μ_e ratio of 2 as compared to the PTB7-

Th:N2200 blend. We note that the balanced hole and electron mobility can reduce bimolecular recombination in the solar cells and thus maximize the photocurrent, which agrees well with the higher J_{sc} of PTB7-Th:PNDI-T10 solar cells.[26] SA on PTB7-Th:PNDI-T10 enables further enhancement in both hole and electron mobilities, reaching the most balanced μ_h/μ_e of 1.7 among all the blends. Since FF values of PSCs correlate with charge transport mobility and the balance of μ_h and μ_e, the enhanced and balanced mobility could explain the increase of FF after SA in the PTB7-Th:PNDI-T10 solar cells.

To further investigate molecular disorder-induced nanostructure variations in the blend films, grazing incidence wide-angle X-ray scattering (GIWAXS) measurements were performed on the PTB7-Th:PNDI-Tx and PTB7-Th:N2200 blends as well as the neat polymers.[27] All the blend films were prepared at the optimized device conditions. Figure S6 in SI shows the 2D GIWAXS images of the neat polymer and blend films. The in-plane and out-of-plane line cuts of GIWAXS patterns are depicted in Figure 4. The neat PTB7-Th and N2200 films show
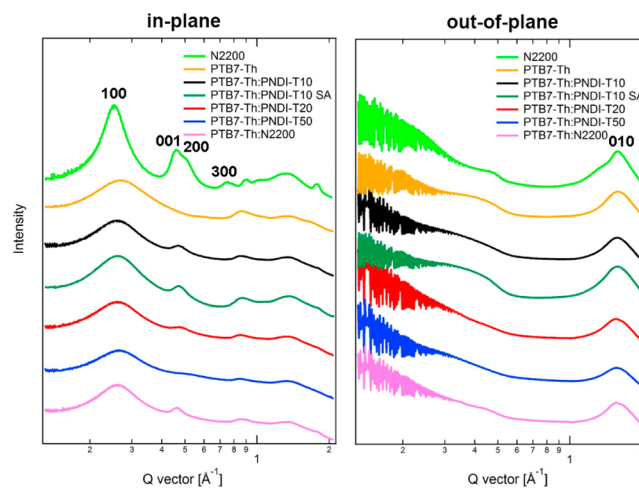
Figure 4. In-plane and out-of-plane line cuts of GIWAXS patterns of PTB7-Th:PNDI-Tx and PTB7-Th:N2200 blend films.

distinct (100) peaks at $q \approx 0.27$ and 0.25 Å^{-1} along the in-plane direction, and (010) peaks at $q \approx 1.59$ and 1.60 Å^{-1} along the out-of-plane direction, respectively. The sharp (100), (001) and (200) peaks of the neat N2200 film indicate a significantly higher degree of crystallization compared to the neat PTB7-Th and PTB7-Th:PNDI-Tx blend films. Each of the blend films only show one broad (100) peak at $q \approx 0.27$ Å^{-1} along the in-plane direction and one (010) peak at $q \approx 1.58$ Å^{-1} along the out-of-plane direction, respectively. This suggests that the two polymers have predominant face-on orientation in all the blends, where the polymer backbones are well aligned with the substrate. Similar face-on orientation of N2200 was also observed in PTB7:N2200 blends.[14a] Very small (001) or/and (200) peaks are only observed in the PTB7-Th:PNDI-T10 and PTB7-Th:N2200 blends, and this peak increases a little in the solvent annealed PTB7-Th:PNDI-T10 blend. It reveals that the increased backbone disorder suppresses the crystallization in the blends, whereas the SA enhances it instead. In order to compare the π−π stacking characteristics of two polymers in the charge transport direction, the (010) coherence length (CL) was revealed by GIWAXS (010) peaks and calculated using the Scherrer equation.[28] Since the (010) peaks of the donor and acceptor polymers totally overlap, the contribution
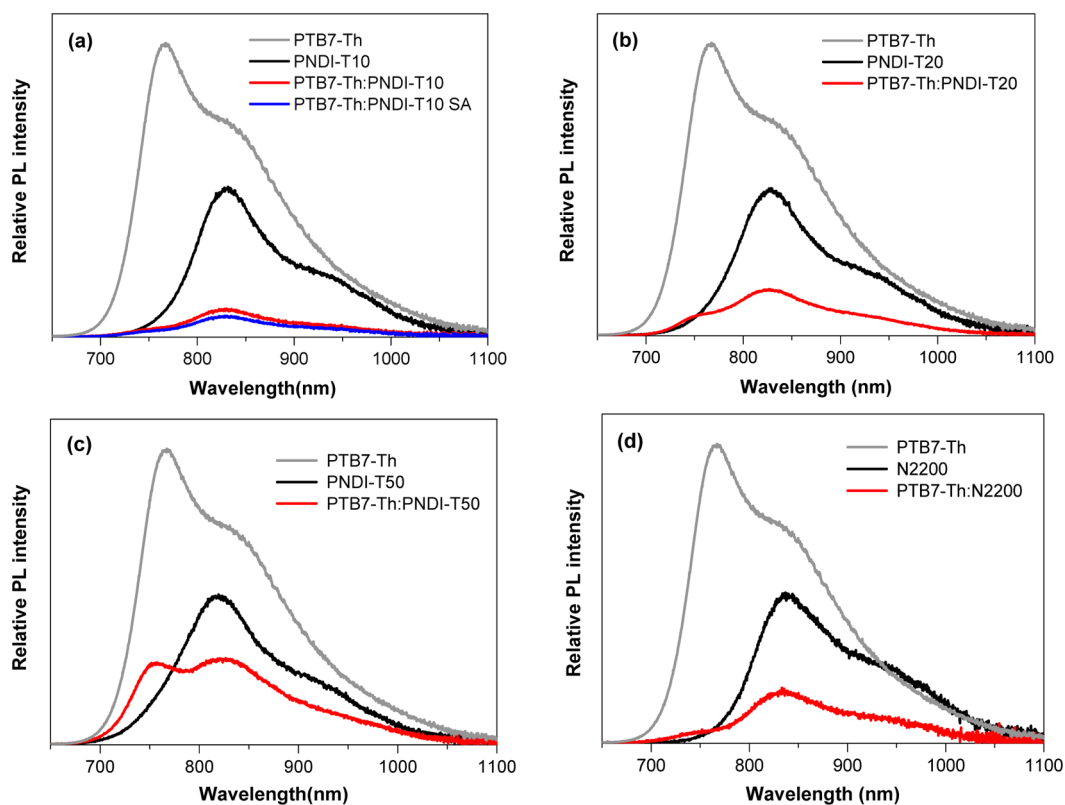
Figure 5. PL spectra obtained from the blend films of (a) PTB7-Th:PNDI-T10 (1:1 w:w); (b) PTB7-Th:PNDI-T20 (1:1 w:w); (c) PTB7-Th:PNDI-T50 (1:1 w:w); and (d) PTB7-Th:N2200 (1:1 w:w) blends.

of each component to the crystallinity is hard to distinguish. In this case, the domains in the blends are composed of a mixture of small crystallites as well as amorphous regions from both the donor and acceptor polymers. As summarized in Table S2 in SI, the PTB7-Th:N2200 blend shows a CL value of 1.96 nm. SA increases the CL value from 1.90 to 2.05 nm in the PTB7-Th:PNDI-T10 blends. Inclusion of 10% thiophene in the N2200 backbone maintains comparable $\pi-\pi$ stacking length with that in the PTB7-Th:N2200 blend. SA further extends the $\pi-\pi$ stacking and enables higher percentage of crystalline regions possibly due to the more flexible backbones of PNDI-T10, which permits molecular chain rearrangement upon SA. In contrast, the PTB7-Th:PNDI-T20 and PTB7-Th:PNDI-T50 blends exhibits much lower CL values around 1.6 nm, indicating the degrees of polymer ordering is prevented when including more disorder in the acceptor backbones. The changes in (010) CL largely parallel the differences in SCLC charge carrier mobilities measured in these blends.

In order to characterize the microscopic phase separation in the blends, we compare the resonant soft X-ray scattering (R-SoXS) results of PTB7-Th:PNDI-Tx and PTB7-Th:N2200 blends at the same condition. Figure S7 in SI shows the R-SoXS scattering profiles of all the blends acquired at 285.2 eV, where the peaks present the domain spacing at $d = 2\pi/q$.[29] For the PTB7-Th:PNDI-T20 and PTB7-Th:PNDI-T50 blends, the low scattering peaks at $q \approx 0.017$ nm^{-1} and 0.025 nm^{-1} correspond to very large domain sizes of 181 and 122 nm, respectively, indicating large phase separation exists in the two blends. In contrast, for the PTB7-Th:PNDI-T10 and PTB7-Th:N2200 blends, the low q peaks at 0.036 and 0.056 nm^{-1} reflect much smaller domain sizes of 87 and 56 nm, respectively. In this case, the best solar cell (PTB7-Th:PNDI-T10) shows a medium

domain size. For polymer:PC$_{71}$BM blends, it has proof that the blend morphology may comprise three phases, a pure and aggregated polymer phase, pure and aggregated PC$_{71}$BM domains, and a mixed amorphous region of the polymer and PC$_{71}$BM.[29b] Although a certain domain size (3–30 nm) is favorable for exciton diffusion to polymer:polymer or polymer:PC$_{71}$BM interfaces,[30] the mixed amorphous region between the two polymer domains is another important factor.[31] In order to evaluate the average composition variations in this mixed amorphous region, the relative average domain purity was calculated from the integration of total scattering intensity (TSI).[29a] Both PTB7-Th:PNDI-T20 and PTB7-Th:PNDI-T50 blends have comparable relative domain purity of 0.83, which are on the low side. There was evidence that relatively low domain purity leads to low mobility and large bimolecular recombination, since the highly mixed two phases in the amorphous region may have less efficient pathways for charge transport.[32] On the other hand, the PTB7-Th:N2200 blend has the purest domains, which is set to 1 as a reference. If the domains are too pure and the sizes are far larger than the exciton diffusion length, typically 10–20 nm,[30] limited D/A interface pathways would lead to poor exciton dissociation.[29b] Therefore, it is worth considering that the average domain purity may have a threshold value in different D/A systems to maximize the performance.[29b,33] The PTB7-Th:PNDI-T10 blend shows a medium domain size and relative domain purity (0.90) among those from PTB7-Th:N2200, PTB7-Th:PNDI-T20 and PTB7-Th:PNDI-T50. In this case, the proper interpenetrating networks between the two pure polymer domains and in the mixed amorphous regions may benefit for the exciton dissociation and charge transport.[34] The morphology study agrees well with the observation in the thermal
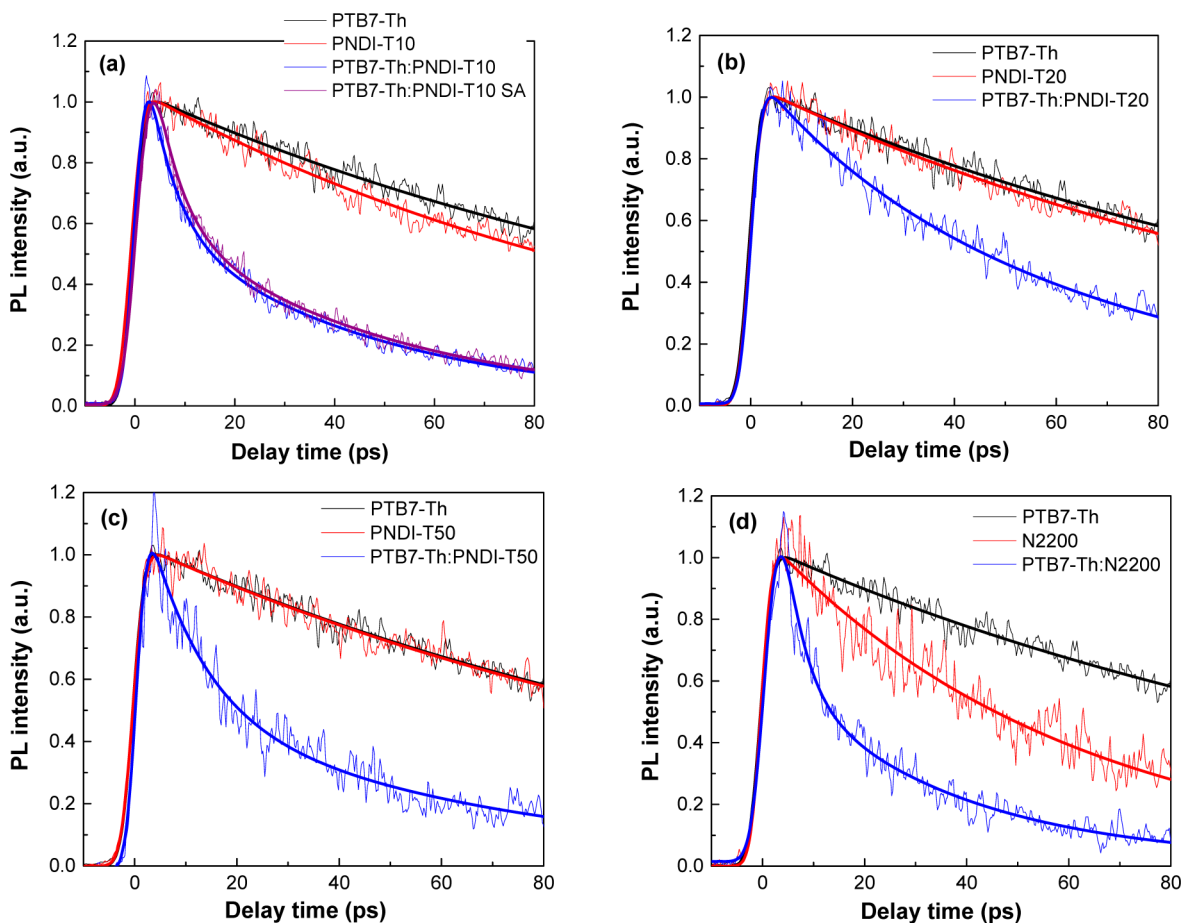
Figure 6. Kinetic traces for neat and blend films of (a) PTB7-Th:PNDI-T10; (b) PTB7-Th:PNDI-T20; (c) PTB7-Th:PNDI-T50; (d) PTB7-Th:N2200 at 830 nm.

property measurements and can explain the difference in hole and electron mobilities of the blends.

To study the surface nanostructure and a qualitative analysis of the phase separation of the blends, atomic force microscopy (AFM) was performed. As shown in Figure S8 in SI, AFM images of PTB7-Th:PNDI-T20 and PTB7-Th:PNDI-T50 show the presence of large aggregates with high root-mean-square (RMS) roughness of 3.6 and 2.8 nm, respectively, which are consistent with the observed large domains in R-SoXS measurements. Both the PTB7-Th:PNDI-T10 and the PTB7-Th:N2200 blends present finer microstructures and continuous phase-segregated morphologies with lower roughness of 1.01 and 1.06 nm, respectively. After SA, the PTB7-Th:PNDI-T10 blend yields the minimal roughness of 0.76 nm, suggesting SA does change the surface of the blend.

Photoluminescence (PL) quenching measurements were performed to investigate exciton diffusion and dissociation in blend films. The steady-state PL spectra of the neat PTB7-Th, PNDI-Tx, N2200 and the corresponding blend films are depicted in Figure 5. The steady-state PL quenching efficiency (ΔPL) was estimated by the PL intensity of the PTB7-Th:acceptor blends relative to that of the neat polymers. The ΔPL reflects the efficiency of exciton diffusion and dissociation at the D/A interface, which gives insight into the nanoscale morphology and polymer miscibility. The PL emission peaks of the neat polymer PTB7-Th and the acceptor polymers are around 766 and 831 nm, respectively. As summarized in Table S3 in SI, the ΔPL of PTB7-Th (ΔPL$_D$) in the PTB7-Th:N2200

and PTB7-Th:PNDI-Tx blends (1:1 w:w) are above 90%, except for the PTB7-Th:PNDI-T50 blend (75%) due to its large phase separation. For the ΔPL of each acceptor (ΔPL$_A$) in the blends, the PL emission of PNDI-T10 is almost quenched in the PTB7-Th:PNDI-T10 blend with the ΔPL$_A$ of 80%. Upon SA, the ΔPL$_A$ further increases to 87%. The higher ΔPL$_D$ and ΔPL$_A$ indicate that more efficient charge transfer occurs due to optimal polymer miscibility in this blend. In contrast, the PL emission of the PTB7-Th:PNDI-T50 blend shows two clear peaks at 756 and 825 nm, which can be attributed to the PL emission from the PTB7-Th and PNDI-T50, respectively. The lower ΔPL$_D$ and ΔPL$_A$ in the PTB7-Th:PNDI-T50 blend indicate inefficient exciton diffusion and dissociation and thus partially explain its low photovoltaic performance. The ΔPL of the PTB7-Th:PNDI-T20 and PTB7-Th:N2200 blends are between those of PTB7-Th:PNDI-T10 and PTB7-Th:PNDI-T50, which is consistent with their modest photovoltaic performance.

In order to investigate ultrafast charge transfer processes occurring within the time scale of picoseconds, we conducted the time-resolved photoluminescence (TRPL) measurements after excited at 400 nm. The blend films were prepared under the optimized device conditions. The normalized spectra are shown in Figure 6 and the lifetime (τ) and quenching efficiency (η) are summarized in Table S4 in SI. The neat PNDI-Tx polymers show longer (>100 ps) PL lifetimes compared to N2200 (59 ps), which is in favor of the diffusion of excitons in the acceptor phase. The quenching efficiency of the donor (η_D)
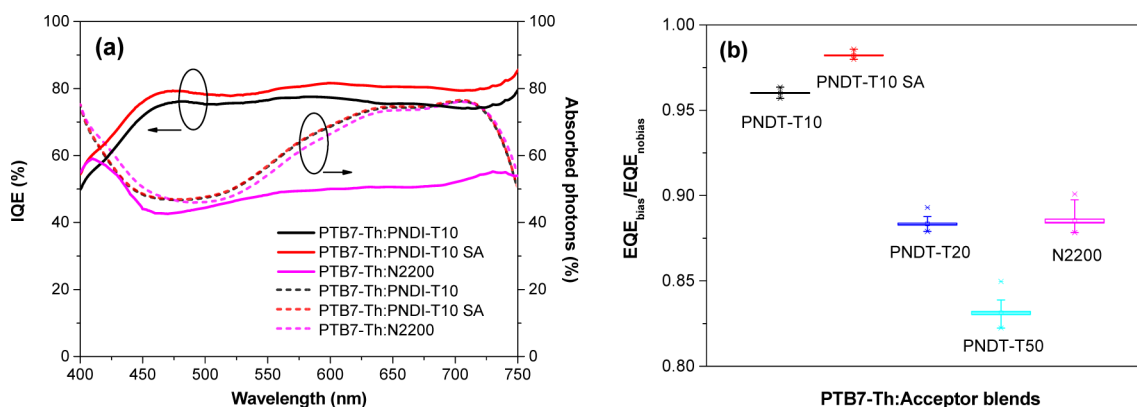
Figure 7. (a) Internal quantum efficiency (IQE) of PTB7-Th:PNDI-T10 and PTB7-Th:N2200 solar cells (solid line). The total absorption of PTB7-Th:PNDI-T10 and PTB7-Th:N2200 blends (dashed line). (b) Average EQE_{bias}/EQE_{nobias} values of PTB7-Th:PNDI-Tx and PTB7-Th:N2200 blends with and without bias light of a 532 nm laser.

in both PTB7-Th:N2200 and PTB7-Th:PNDI-T10 blends reach very high value of ~96%. It suggests that the exciton generated in the donor PTB7-Th can efficiently dissociate at the D/A interface. On the other hand, the quenching efficiency of the acceptor (η_A) in the PTB7-Th:PNDI-T10 blend is 72%, higher than that of 63% in the PTB7-Th:N2200 blend. The higher η_A demonstrates that the charges generated in the acceptor PNDI-T10 contribute more to the total photocurrent compared to N2200, which is consistent with the EQE profiles and the longer PL lifetime of PNDI-T10. The values of η_D and η_A in the PTB7-Th:PNDI-T10 blend have no variation after SA, which indicates that the enhanced FF of this blend may not benefit from the exciton dissociation process. For those blends presenting larger phase separation, the PTB7-Th:PNDI-T20 and PTB7-Th:PNDI-T50 blends show lower quenching efficiency both on the donor and acceptor side. The exciton dissociation is significantly limited by the undesired nanostructures in the two blends. The PL quenching behavior of the TRPL measurements agrees well with the steady-state PL measurements discussed above. Both the steady-state PL and TRPL results agree with the blend morphology, molecule orientation and phase-separation measurements using AFM, GIWAXS and R-SoXS, where the PTB7-Th:PNDI-T10 blend has more extended $\pi-\pi$ stacking in the direction of charge transport and presents optimal phase-separation with medium domain purity. These are in favor of more efficient exciton diffusion and dissociation compared to other polymer:polymer blends.

To evaluate the efficiency of collected carriers per incident absorbed photon, the internal quantum efficiency (IQE) was determined from the EQE of the PTB7-Th:PNDI-T10 and PTB7-Th:N2200 solar cells and the total fraction of absorbed photons. The latter was calculated from the wavelength-dependent refractive index (n) and extinction coefficient (k) of all layers via optical modeling of the entire layer stack. As shown in Figure 7a and Figure S9 in SI, SA leads to a slightly IQE increase of PTB7-Th:PNDI-T10 solar cells. The IQE (red line) stays near or even above 80% throughout the entire absorption spectrum (400−750 nm), which is rarely observed in all-PSCs. In contrast, the PTB7-Th:N2200 solar cell shows much lower IQE of around 50%. The higher IQE of PTB7-Th:PNDI-T10 solar cell confirms that the absorbed photons are efficiently converted into charge carriers and collected at the electrodes.

In addition, we studied the charge recombination mechanism in these all-PSCs. Figure S10 in SI depicts the J−V and EQE characterization of PTB7-Th:PNDI-T10 solar cell under bias voltages. The EQE profiles present no obvious variation when the reverse bias voltage of −2 V is applied and the quick saturation of the photocurrent under bias voltage is rare to see in all-PSCs,[12b] suggesting that the intrinsic driving force is sufficient to sweep out most of the free charges to the electrodes, and bimolecular recombination is negligible in the PTB7-Th:PNDI-T10 blend. In this case, the charge recombination loss may only stem from the geminate recombination rather than bimolecular recombination.[12b,26] In order to quantify the bimolecular recombination losses, the EQE profiles with or without the illumination of bias light at a wavelength of 530 nm were measured (Figure S11 in SI). Since bimolecular recombination strongly depends on the charge carrier density, an extra bias illumination would increase charge carrier density in the devices and boost bimolecular recombination, and in turn reduce the EQE. Therefore, the ratio between the measured EQE with and without bias light (EQE_{bias}/EQE_{nobias}) quantitatively reflects the bimolecular recombination characteristics. The EQE_{bias}/EQE_{nobias} ratio is a more precise way of determining the light intensity dependence than simply measuring the J_{sc} as a function of light intensity.[35] The bimolecular recombination efficiency (η_{BR}) is denoted by $\eta_{BR} = EQE_{nobias}/EQE_{bias} − 1$, where a low η_{BR} value suggests negligible bimolecular recombination.[35] As shown in Figure 7b, the PTB7-Th:PNDI-T10 blend shows much lower η_{BR} of 0.04 compared to those of other blends, implying negligible bimolecular recombination exists in this blend. After SA, the bimolecular recombination is further reduced, since the η_{BR} attains to the minimum of 0.02. As the bimolecular recombination is determined by the rate at which oppositely charged carriers meet one another, it would be suppressed by the high and balanced charge carrier mobilities in this solvent annealed PTB7-Th:PNDI-T10 blend.[26] The negligible bimolecular recombination indicates the electrodes can collect all the separated charges when the mobility of the blend is on the order of 10^{-4} cm^2 V^{-1} s^{-1}, which has not been observed in all-PSCs before. For the PTB7-Th:PNDI-T20 and PTB7-Th:PNDI-T50 blends, much larger η_{BR} of 0.14 and 0.17 were observed, respectively, which is probably due to their large phase separation as indicated by R-SoXS. The quantitative analysis of the bimolecular recombination is also consistent with the charge transporting properties, where the high and

balanced electron and hole mobilities can prevent significant bimolecular recombination, and boost the photovoltaic performance.

■ CONCLUSIONS

In summary, we synthesized a series of NDI-bithiophene-thiophene random polymers (PNDI-Tx) with the intention to fine-tune the crystallinity and nanostructures of the resulting donor:acceptor blends. Upon varying the content of thiophene units, this simple strategy gradually reduces the crystallinity and largely improves the solubility and thus molecular weights of the random polymers. The polymer PNDI-T10 shows optimal miscibility with the donor PTB7-Th and balanced hole and electron mobility in the blend, which leads to the best performance with a high PCE of 7.6% and a decent FF of 0.71 for the solar cells with a device area of 16 mm^2. It is found that the bimolecular recombination of this all-PSC is negligible such that virtually all separated charges can be efficiently transported and collected by electrodes, which is not observed in all-PSCs to date. Gratifyingly, the remarkably high FF is the highest value among all-PSCs and overcomes one of the main limiting factors, which restricted the efficiency of all-PSCs for a long time. It doubtlessly reflects the bright future of all-PSCs. Using this simply synthetic strategy, the random polymer PNDI-T10 proves to be a promising alternative to the commercial polymer N2200 to provide superior performance in all-PSCs.

■ ASSOCIATED CONTENT

ⓢ Supporting Information

The Supporting Information is available free of charge on the ACS Publications website at DOI: 10.1021/jacs.6b04822.

> Synthesis and characterizations, DSC measurements, optical and electrochemical properties, All-PSCs fabrication, characterization and optimization, SCLC measurements, GIWAXS and R-SoXS measurements, AFM images, steady-state PL and TRPL measurements, IQE measurements, EQE characteristics under bias voltages and bias light. (PDF)

■ AUTHOR INFORMATION

Corresponding Authors
*xixu@chalmers.se
*r.a.j.janssen@tue.nl
*ergang@chalmers.se

Notes
The authors declare no competing financial interest.

■ ACKNOWLEDGMENTS

■ REFERENCES

(1) Heeger, A. J. *Adv. Mater.* **2014**, *26*, 10−28.

(2) Wang, E.; Mammo, W.; Andersson, M. R. *Adv. Mater.* **2014**, *26*, 1801−1826.

(3) Zhao, J.; Li, Y.; Yang, G.; Jiang, K.; Lin, H.; Ade, H.; Ma, W.; Yan, H. *Nat. Energy* **2016**, *1*, 15027.

(4) Facchetti, A. *Mater. Today* **2013**, *16*, 123−132.

(5) (a) Gao, L.; Zhang, Z.-G.; Xue, L.; Min, J.; Zhang, J.; Wei, Z.; Li, Y. *Adv. Mater.* **2016**, *28*, 1884−1890. (b) Bin, H.; Zhang, Z.-G.; Gao, L.; Chen, S.; Zhong, L.; Xue, L.; Yang, C.; Li, Y. *J. Am. Chem. Soc.* **2016**, *138*, 4657−4664.

(6) (a) Lin, Y.; Zhan, X. *Mater. Horiz.* **2014**, *1*, 470−488. (b) Nielsen, C. B.; Holliday, S.; Chen, H.-Y.; Cryer, S. J.; McCulloch, I. *Acc. Chem. Res.* **2015**, *48*, 2803−2812. (c) Kang, H.; Uddin, M. A.; Lee, C.; Kim, K.-H.; Nguyen, T. L.; Lee, W.; Li, Y.; Wang, C.; Woo, H. Y.; Kim, B. J. *J. Am. Chem. Soc.* **2015**, *137*, 2359−2365. (d) Zhou, N.; Dudnik, A. S.; Li, T. I. N. G.; Manley, E. F.; Aldrich, T. J.; Guo, P.; Liao, H.-C.; Chen, Z.; Chen, L. X.; Chang, R. P. H.; Facchetti, A.; Olvera de la Cruz, M.; Marks, T. J. *J. Am. Chem. Soc.* **2016**, *138*, 1240−1251.

(7) (a) Liu, X.; Huettner, S.; Rong, Z.; Sommer, M.; Friend, R. H. *Adv. Mater.* **2012**, *24*, 669−674. (b) Mori, D.; Benten, H.; Ohkita, H.; Ito, S.; Miyake, K. *ACS Appl. Mater. Interfaces* **2012**, *4*, 3325−3329. (c) Cao, Y.; Lei, T.; Yuan, J. S.; Wang, J. Y.; Pei, J. *Polym. Chem.* **2013**, *4*, 5228−5236.

(8) (a) Li, W.; Roelofs, W. S.; Turbiez, M.; Wienk, M. M.; Janssen, R. A. *Adv. Mater.* **2014**, *26*, 3304−3309. (b) Li, W. W.; An, Y.; Wienk, M. M.; Janssen, R. A. *J. Mater. Chem. A* **2015**, *3*, 6756−6760.

(9) Bhosale, S. V.; Jani, C. H.; Langford, S. J. *Chem. Soc. Rev.* **2008**, *37*, 331−342.

(10) Seo, J. H.; Gutacker, A.; Sun, Y.; Wu, H.; Huang, F.; Cao, Y.; Scherf, U.; Heeger, A. J.; Bazan, G. C. *J. Am. Chem. Soc.* **2011**, *133*, 8416−8419.

(11) (a) Yan, H.; Chen, Z.; Zheng, Y.; Newman, C.; Quinn, J. R.; Dotz, F.; Kastler, M.; Facchetti, A. *Nature* **2009**, *457*, 679−686. (b) Schuettfort, T.; Huettner, S.; Lilliu, S.; Macdonald, J. E.; Thomsen, L.; McNeill, C. R. *Macromolecules* **2011**, *44*, 1530−1539. (c) Fabiano, S.; Musumeci, C.; Chen, Z.; Scandurra, A.; Wang, H.; Loo, Y.-L.; Facchetti, A.; Pignataro, B. *Adv. Mater.* **2012**, *24*, 951−956.

(12) (a) Luzio, A.; Criante, L.; D'Innocenzo, V.; Caironi, M. *Sci. Rep.* **2013**, *3*, 3425. (b) Mori, D.; Benten, H.; Okada, I.; Ohkita, H.; Ito, S. *Energy Environ. Sci.* **2014**, *7*, 2939−2943. (c) Steyrleuthner, R.; Di Pietro, R.; Collins, B. A.; Polzer, F.; Himmelberger, S.; Schubert, M.; Chen, Z.; Zhang, S.; Salleo, A.; Ade, H.; Facchetti, A.; Neher, D. *J. Am. Chem. Soc.* **2014**, *136*, 4245−4256. (d) Mori, D.; Benten, H.; Okada, I.; Ohkita, H.; Ito, S. *Adv. Energy Mater.* **2014**, *4*, 1301006.

(13) Schubert, M.; Dolfen, D.; Frisch, J.; Roland, S.; Steyrleuthner, R.; Stiller, B.; Chen, Z.; Scherf, U.; Koch, N.; Facchetti, A.; Neher, D. *Adv. Energy Mater.* **2012**, *2*, 369−380.

(14) (a) Zhou, N.; Lin, H.; Lou, S. J.; Yu, X.; Guo, P.; Manley, E. F.; Loser, S.; Hartnett, P.; Huang, H.; Wasielewski, M. R.; Chen, L. X.; Chang, R. P. H.; Facchetti, A.; Marks, T. J. *Adv. Energy Mater.* **2014**, *4*, 1300785. (b) Mu, C.; Liu, P.; Ma, W.; Jiang, K.; Zhao, J.; Zhang, K.; Chen, Z.; Wei, Z.; Yi, Y.; Wang, J.; Yang, S.; Huang, F.; Facchetti, A.; Ade, H.; Yan, H. *Adv. Mater.* **2014**, *26*, 7224−7230. (c) Shi, G.; Yuan, J.; Huang, X.; Lu, Y.; Liu, Z.; Peng, J.; Ding, G.; Shi, S.; Sun, J.; Lu, K.; Wang, H.-Q.; Ma, W. *J. Phys. Chem. C* **2015**, *119*, 25298−25306. (d) Tang, Z.; Liu, B.; Melianas, A.; Bergqvist, J.; Tress, W.; Bao, Q.;

Qian, D.; Inganäs, O.; Zhang, F. *Adv. Mater.* **2015**, *27*, 1900−1907. (e) Yuan, J.; Ma, W. *J. Mater. Chem. A* **2015**, *3*, 7077−7085. (f) Xia, Y.; Musumeci, C.; Bergqvist, J.; Ma, W.; Gao, F.; Tang, Z.; Bai, S.; Jin, Y.; Zhu, C.; Kroon, R.; Wang, C.; Andersson, M. R.; Hou, L.; Inganäs, O.; Wang, E. *J. Mater. Chem. A* **2016**, *4*, 3835−3843.

(15) (a) Hwang, Y.-J.; Earmme, T.; Subramaniyan, S.; Jenekhe, S. A. *Chem. Commun.* **2014**, *50*, 10801−10804. (b) Hwang, Y. J.; Earmme, T.; Courtright, B. A.; Eberle, F. N.; Jenekhe, S. A. *J. Am. Chem. Soc.* **2015**, *137*, 4424−4434. (c) Dai, S.; Cheng, P.; Lin, Y.; Wang, Y.; Ma, L.; Ling, Q.; Zhan, X. *Polym. Chem.* **2015**, *6*, 5254−5263.

(16) He, Z.; Xiao, B.; Liu, F.; Wu, H.; Yang, Y.; Xiao, S.; Wang, C.; Russell, T. P.; Cao, Y. *Nat. Photonics* **2015**, *9*, 174−179.

(17) Wunderlich, B. *Pure Appl. Chem.* **1995**, *67*, 1019−1026.

(18) Alsleben, M.; Schick, C. *Thermochim. Acta* **1994**, *238*, 203−227.

(19) (a) Earmme, T.; Hwang, Y. J.; Subramaniyan, S.; Jenekhe, S. A. *Adv. Mater.* **2014**, *26*, 6080−6085. (b) Hwang, Y. J.; Ren, G. Q.; Murari, N. M.; Jenekhe, S. A. *Macromolecules* **2012**, *45*, 9056−9062.

(20) Kim, T.; Kim, J.-H.; Kang, T. E.; Lee, C.; Kang, H.; Shin, M.; Wang, C.; Ma, B.; Jeong, U.; Kim, T.-S.; Kim, B. J. *Nat. Commun.* **2015**, *6*, 8547.

(21) Ren, G.; Schlenker, C. W.; Ahmed, E.; Subramaniyan, S.; Olthof, S.; Kahn, A.; Ginger, D. S.; Jenekhe, S. A. *Adv. Funct. Mater.* **2013**, *23*, 1238−1249.

(22) (a) Choi, J.; Kim, K. H.; Yu, H.; Lee, C.; Kang, H.; Song, I.; Kim, Y.; Oh, J. H.; Kim, B. J. *Chem. Mater.* **2015**, *27*, 5230−5237. (b) Zhou, K.; Zhang, R.; Liu, J.; Li, M.; Yu, X.; Xing, R.; Han, Y. *ACS Appl. Mater. Interfaces* **2015**, *7*, 25352−25361.

(23) Hwang, Y.-J.; Courtright, B. A. E.; Ferreira, A. S.; Tolbert, S. H.; Jenekhe, S. A. *Adv. Mater.* **2015**, *27*, 4578−4584.

(24) Lee, C.; Kang, H.; Lee, W.; Kim, T.; Kim, K.-H.; Woo, H. Y.; Wang, C.; Kim, B. J. *Adv. Mater.* **2015**, *27*, 2466−2471.

(25) Müller, C.; Wang, E.; Andersson, L. M.; Tvingstedt, K.; Zhou, Y.; Andersson, M. R.; Inganäs, O. *Adv. Funct. Mater.* **2010**, *20*, 2124−2131.

(26) Proctor, C. M.; Kuik, M.; Nguyen, T.-Q. *Prog. Polym. Sci.* **2013**, *38*, 1941−1960.

(27) Tumbleston, J. R.; Collins, B. A.; Yang, L.; Stuart, A. C.; Gann, E.; Ma, W.; You, W.; Ade, H. *Nat. Photonics* **2014**, *8*, 385−391.

(28) Smilgies, D.-M. *J. Appl. Crystallogr.* **2013**, *46*, 286.

(29) (a) Collins, B. A.; Li, Z.; Tumbleston, J. R.; Gann, E.; McNeill, C. R.; Ade, H. *Adv. Energy Mater.* **2013**, *3*, 65−74. (b) Ma, W.; Tumbleston, J. R.; Wang, M.; Gann, E.; Huang, F.; Ade, H. *Adv. Energy Mater.* **2013**, *3*, 864−872.

(30) (a) Pavlopoulou, E.; Kim, C. S.; Lee, S. S.; Chen, Z. H.; Facchetti, A.; Toney, M. F.; Loo, Y. L. *Chem. Mater.* **2014**, *26*, 5020−5027. (b) Bartelt, J. A.; Beiley, Z. M.; Hoke, E. T.; Mateker, W. R.; Douglas, J. D.; Collins, B. A.; Tumbleston, J. R.; Graham, K. R.; Amassian, A.; Ade, H.; Frechet, J. M. J.; Toney, M. F.; McGehee, M. D. *Adv. Energy Mater.* **2013**, *3*, 364−374. (c) Sweetnam, S.; Graham, K. R.; Ngongang Ndjawa, G. O.; Heumuller, T.; Bartelt, J. A.; Burke, T. M.; Li, W.; You, W.; Amassian, A.; McGehee, M. D. *J. Am. Chem. Soc.* **2014**, *136*, 14078−14088.

(31) Mukherjee, S.; Proctor, C. M.; Tumbleston, J. R.; Bazan, G. C.; Nguyen, T.-Q.; Ade, H. *Adv. Mater.* **2015**, *27*, 1105−1111.

(32) Albrecht, S.; Janietz, S.; Schindler, W.; Frisch, J.; Kurpiers, J.; Kniepert, J.; Inal, S.; Pingel, P.; Fostiropoulos, K.; Koch, N.; Neher, D. *J. Am. Chem. Soc.* **2012**, *134*, 14932−14944.

(33) Ma, W.; Tumbleston, J. R.; Ye, L.; Wang, C.; Hou, J.; Ade, H. *Adv. Mater.* **2014**, *26*, 4234−4241.

(34) Ye, L.; Jiao, X.; Zhou, M.; Zhang, S.; Yao, H.; Zhao, W.; Xia, A.; Ade, H.; Hou, J. *Adv. Mater.* **2015**, *27*, 6046−6054.

(35) (a) Koster, L. J. A.; Kemerink, M.; Wienk, M. M.; Maturová, K.; Janssen, R. A. J. *Adv. Mater.* **2011**, *23*, 1670−1674. (b) Wehenkel, D. J.; Hendriks, K. H.; Wienk, M. M.; Janssen, R. A. J. *Org. Electron.* **2012**, *13*, 3284−3290.